MODELLISTICA E CALCOLO SCIENTIFICO

MOX

MODELING AND SCIENTIFIC COMPUTING

Semi-Automatic Three-Dimensional Vessel Segmentation Using a Connected Component Localization of the Region-Scalable Fitting Energy

Fedele, M.; Faggiano, E.; Barbarotta, L.; Cremonesi, F.;

Formaggia, L.; Perotto, S.

MOX, Dipartimento di Matematica
Politecnico di Milano, Via Bonardi 9 - 20133 Milano (Italy)

mox-dmat@polimi.it   http://mox.polimi.it

Semi-Automatic Three-Dimensional Vessel Segmentation Using a Connected Component Localization of the Region-Scalable Fitting Energy

Marco Fedele[*†], Elena Faggiano[*†], Luca Barbarotta[†],
Francesco Cremonesi[†], Luca Formaggia[†] and Simona Perotto[†]

July 9, 2015

[*] Computational Mechanics & Advanced Materials Group
Dipartimento di Ingegneria Civile e Architettura,
Università di Pavia, Pavia, Italy
Via Ferrata, 3, 27100 Pavia, Italy

[†]MOX – Modellistica e Calcolo Scientifico
Dipartimento di Matematica "F. Brioschi"
Politecnico di Milano
via Bonardi 9, 20133 Milano, Italy

elena.faggiano@gmail.com

Abstract

Segmentation of patient-specific vascular segments of interest from medical images is an important topic for numerous applications. Despite the great importance of having semi-automatic segmentation methods in this field, the process of image segmentation is still based on several operator-dependent steps which make large-scale segmentation a non trivial and time consuming task. In this work we present a semi-automatic segmentation method to reconstruct vascular structures from three-dimensional medical images. We start from the minimization of the Region Scalable Fitting Energy using the Split-Bregman method and we modify the resulting algorithm adding a connected component extraction of the solution starting from a point that identifies the vascular structure of interest. In this way, we add a constraint to the algorithm focusing it only on the vascular structure we want to reconstruct and avoiding the attachment with the nearby objects. Finally, we describe a strategy to minimize the number of involved parameters in order to limit the user effort. The results obtained on

two different images (a Magnetic Resonance and a Computed Tomography) demonstrate that our method outperforms the original method in segmenting the vascular region of interest without the inclusion of nearby objects in the result.

1 Introduction

Segmentation of patient-specific vascular segments of interest from medical images is an important topic for numerous applications such as patient-specific computational hemodynamics [1], patient-specific computational mechanics [2] and patient-specific complex vascular morphological analysis [3, 4]. Despite the amount of studies concerning the aforementioned fields has been growing over the last years, works including a large patient population are still very limited [3, 5]. The ability of performing large-scale studies in a controlled way is a fundamental requirement in the clinical setting. Indeed, only large-scale studies can be used to draw population conclusions or to validate computational methods. One of the main reasons for the lack of large studies is the fact that, starting from medical images, the process of image segmentation is still based on several operator-dependent steps which make large-scale segmentation a non trivial and time consuming task. Moreover, operator-dependent tasks represent a source of error difficult to quantify. The semi-automatic tools that are able to segment vascular structures with low user interaction are few [6, 7] and still require a certain amount of user involvement. In Antiga *et al.* [7], for example, the segmentation algorithm requires the user to put two seeds for each branch of the vascular segment to be segmented. This implies that, for complex geometries such as the aorta or the coronaries, the user should define six or more initial seeds with a consequent user effort in image interpretation. Starting from these considerations, in this work we aim to propose a new segmentation method for vascular structure able to: (i) work on different types of medical images (e.g. Magnetic Resonance images, Computed Tomography scans), (ii) minimize user interaction and operator dependence, (iii) minimize the number of parameters to be specified. To this aim we develop a region based segmentation method which includes a local constraint able to extract only a user-defined region of interest, avoiding its attachment with nearby regions. Moreover, we reduce the user effort to the selection of a single initial point and to the setting of only three parameters. The method is developed in C++ using some of the structures provided by The Visualization Toolkit (*www.vtk.org*) for the visualization and the interaction with the user.

2 Methods

The anatomy of blood vessels can be inferred from Magnetic resonance (MR) studies, three dimensional ultrasound (3D-US), computed tomography (CT) and rotational angiography (RA) scanners. The information provided by these clinical scanners is represented as a 3D array of grayscale intensities. In this work we are interested not in the identification of entire vascular networks contained in the image but in the identification of the individual vascular segments of interest. In this way, the result of our segmentation strategy is ready to be used for grid generation for computational analysis or directly for morphological exploration. To this aim we ask to the user the unique identification of a point inside the object of interest limiting the effort required by the operator in the interpretation of the image content. To define our segmentation strategy two main components have to be described: the segmentation method in terms of the involved equations and the choice of the feature image, i.e. the input to the segmentation itself. Our segmentation method starts from the method proposed in [8] which is based on the minimization of the Region-Scalable Fitting Energy (RSFE) [9] through the Split-Bregman method [10]; we further modify the method through the incorporation of an iterative Connected Component [11] extraction. The RSFE model, firstly proposed in [9], can be seen as an improvement of the classical Piecewise Constant Chan-Vese model [12]. In the latest, the image is divided in two regions approximating the intensity of the image inside each region with a constant value representing the average of the intensity inside the region. The idea behind the RSFE model is similar, but it substitutes the constant values with functions that approximate the image intensity in a local region through the use of a Gaussian kernel. The method is scalable because the Gaussian kernel depends on a scale parameter, thus it is possible to decide the size of the stencils on which the average of the intensity around a pixel is calculated. In [8] the original energy is modified to make it convex through the use of the Global Convex Segmentation (GCS) method [13]. In this work we start with the same convex functional proposed in [8] and we modify it adding an iterative Connected Component extraction to deal with the problem of segmentation of an individual region of interest in medical images.

In detail, let $\Omega \subset \mathbb{R}^3$ be the image domain: the aim of the method is to subdivide the domain into two regions Ω_1 and Ω_2 representing the object to be segmented and the background, respectively. The functional $\mathcal{F}$ to be minimized is written in a level set formulation, in this way the zero level of the level set function represents the boundary between Ω_1 and Ω_2. We use the following notation: $u_0 : \Omega \to \mathbb{R}$ is the image intensity function, $\phi : \Omega \to \mathbb{R}$ is the level set function, $L^1(\Omega)$ is the function space of Lebesgue-integrable functions and $\| \cdot \|_1$ is its norm, $L^2(\Omega)$ is the Hilbert space of the square-integrable functions, $\|\cdot\|_2$ is its norm and $\langle \cdot, \cdot \rangle$ is its inner

3

product, $H^1(\Omega) \subset L^2(\Omega)$ is the Hilbert space of the functions with also a square-integrable gradient, $*$ denotes the convolution product. We set the minimization problem in the limited space $\mathcal{U}_{ad}$ to make the global minimum well defined [8]:

$$\mathcal{U}_{ad} := \{\phi \in H^1(\Omega) : \ -\alpha \leq \phi(\boldsymbol{x}) \leq \alpha, \ q.o. \ \boldsymbol{x} \in \Omega\}, \tag{1}$$

$$\phi = \underset{\phi \, \in \, \mathcal{U}_{ad}}{\arg\min} \ \mathcal{F}(\phi), \tag{2}$$

where α is a positive constant. The functional reads:

$$\mathcal{F}(\phi(\boldsymbol{x})) = \langle \phi(\boldsymbol{x}), \lambda_1 e_1(\phi(\boldsymbol{x})) - \lambda_2 e_2(\phi(\boldsymbol{x})) \rangle \tag{3a}$$

$$+ \nu \|\nabla \phi(\boldsymbol{x})\|_g, \qquad \boldsymbol{x} \in \Omega, \tag{3b}$$

where λ_1, λ_2, ν are positive constants and we define the following functions:

$$\mathcal{H}_\varepsilon(\phi(\boldsymbol{x})) = \ 0.5 + \pi^{-1} \arctan\left(\phi(\boldsymbol{x})/\varepsilon\right), \tag{4}$$

$$M_{\varepsilon,1}(\phi(\boldsymbol{x})) = \ \mathcal{H}_\varepsilon\left(\phi(\boldsymbol{x})\right), \tag{5}$$

$$M_{\varepsilon,2}(\phi(\boldsymbol{x})) = \ 1 - \mathcal{H}_\varepsilon\left(\phi(\boldsymbol{x})\right), \tag{6}$$

$$K_\sigma(\boldsymbol{x}) = \ \frac{1}{(\sqrt{2\pi}\sigma)^3} \exp\left\{-\frac{|\boldsymbol{x}|^2}{2\sigma^2}\right\}, \tag{7}$$

$$f_i(\phi(\boldsymbol{x})) = \ \frac{(K_\sigma * M_{\varepsilon,i} u_0)(\boldsymbol{x})}{(K_\sigma * M_{\varepsilon,i})(\boldsymbol{x})}, \quad i = 1, 2 \ , \tag{8}$$

$$e_i(\phi(\boldsymbol{x})) = \ \int_\Omega K_\sigma(\boldsymbol{x} - \boldsymbol{y}) \left|u_0(\boldsymbol{x}) - f_i(\phi(\boldsymbol{y}))\right|^2 d\boldsymbol{y}, \tag{9}$$

$$g(u_0(\boldsymbol{x})) = \ \frac{1}{1 + \beta \left|\nabla(u_o(\boldsymbol{x}))\right|^2}, \quad \beta \in \mathbb{R}^+, \tag{10}$$

$$\|\nabla \phi(\boldsymbol{x})\|_g = \ \|g(u_0(\boldsymbol{x}))\nabla \phi(\boldsymbol{x})\|_1. \tag{11}$$

$\mathcal{H}_\varepsilon$ is a smoothed Heaviside function depending on the smoothing parameter ε and as a consequence the two functions $M_{\varepsilon,i}$ identify the two domains Ω_1 and Ω_2. The regional scalable behavior of the method is due to the presence of the Gaussian kernel K_σ depending on the scaling parameter σ. Combining these functions and u_0 through the convolution product, the functions f_1 and f_2 play the role of a local approximations of the image intensities in Ω_1 and Ω_2, respectively. In conclusion, the first term (3a) in the functional is the term which guides the method to divide the image into two regions. Instead, the second term (3b), as proposed in [8,14], is a modification of the standard total variation norm adding the classical edge detector function $g(u_0)$ as a weight (see equation (10) and (11)). Hence, this term plays the role of a penalization on the smoothness of the segmented region enriched with information about the position of the image edges taken directly from the image intensity function u_0.

4

The application of the Split-Bregman method to solve (2) leads to the following iterative algorithm [8, 10]:

$$\phi^0 = \phi_0, \qquad \boldsymbol{d}^0 = \nabla\phi_0, \qquad \boldsymbol{b}^0 = \boldsymbol{0}, \tag{12a}$$

$$r^k = \lambda_1 e_1(\phi^k) - \lambda_2 e_2(\phi^k), \tag{12b}$$

$$\phi^{k+1} = \underset{\phi \,\in\, \mathcal{U}_{ad}}{\arg\min} \left\{ \langle \phi, r^k \rangle + \frac{\lambda}{2} \left\| \boldsymbol{d}^k - \nabla\phi - \boldsymbol{b}^k \right\|_2^2 \right\}, \tag{12c}$$

$$\boldsymbol{d}^{k+1} = \underset{\boldsymbol{d}}{\arg\min} \left\{ \nu\|\boldsymbol{d}\|_g + \frac{\lambda}{2} \left\| \boldsymbol{d} - \nabla\phi^{k+1} - \boldsymbol{b}^k \right\|_2^2 \right\}, \tag{12d}$$

$$\boldsymbol{b}^{k+1} = \boldsymbol{b}^k + \nabla\phi^{k+1} - \boldsymbol{d}^{k+1}, \tag{12e}$$

where ϕ_0 is the arbitrary initial level set function and λ is a positive constant. The Euler-Lagrange equation of the first optimization problem (12c) leads to the resolution of the following Poisson problem to find ϕ^{k+1}:

$$\begin{cases} -\Delta\phi \;=\; \nabla \cdot \left(\boldsymbol{b}^k - \boldsymbol{d}^k \right) - \dfrac{r^k}{\lambda} & \text{in } \Omega \\[2mm] \partial_{\boldsymbol{n}}\phi \;=\; 0 & \text{on } \partial\Omega \end{cases} , \quad \phi \in \mathcal{U}_{ad}. \tag{13}$$

Note that the definition of r^k in (12b) exploiting the level set ϕ^k of the previous iteration follows the implementation of [8] and it is necessary to obtain in (13) a linear partial differential equation. The minimization of (12d) can be performed, instead, using the shrinkage operator [10]:

$$\text{shrink}(f, \gamma) \;=\; \text{sgn}\, f \; \max(|f| - \gamma,\, 0), \tag{14}$$

which leads

$$\boldsymbol{d}^{k+1} \;=\; \text{shrink} \left(\boldsymbol{b}^k + \nabla\phi^{k+1}, \; \frac{\nu}{\lambda} \, g\left(u_0\left(\phi^{k+1} \right) \right) \right). \tag{15}$$

Concerning our numerical implementation, we discretize each function involved in the algorithm on the structured grid of pixels naturally defined by the 3D medical image. Thus, we use the finite difference method to discretize (13), as well as every other differential operator. Finally, we solve the linear system generated by the finite difference discretization of (13) using the Gauss-Seidel iterative method initializing the solution with the level set at the previous iteration ϕ^k. We solve the convolution products in (8) and (9), necessary to update r^k at each iteration, exploiting the Convolution Theorem and the Discrete Fourier Transform (DFT) of each factor. Moreover, we compute each DFT using the Fast Fourier Transform (FFT) algorithm and, as proposed in [9], we limit to four the number of convolutions necessary at each iteration. Concerning the initialization, we always define the level set ϕ_0 as a small cube including the region of interest of the medical image, assuming the value α inside and $-\alpha$ outside. The cube

5

is constructed asking to the user the identification of one point inside the vessel of interest and a characteristic dimension of the vessel itself.

The method described above is a region-based method that divides the image in two regions. Each region can be constituted of more than a unique connected part. Furthermore, since the second part of the functional (3b) penalizes the curvature of the object to be segmented, the algorithm encourages the union between objects near each other. These are typical limitations when dealing with 3D medical images, since usually in this field the goal of the segmentation is to isolate a single organ of interest from everything else: the attachment of the object of interest with nearby objects with similar intensity is a classical problem. To overcome these problems, we include in our method an automatic Connected Component Extraction (CCE) [11] of the level set ϕ. Since the level set assumes positive values inside the region of interest and negative outside, the CCE consists of selecting only the pixels which have positive values and which are topologically connected to an initial point P_0, chosen inside the region of interest (for example, the center of the initial cube defined by ϕ_0 or a different point chosen by the user). This procedure is performed automatically each N iterations and only if the level set is positive in the initial point P_0. In this case, we define the level set ϕ^{k+1} as a binary image equal to α inside the extracted component and to $-\alpha$ otherwise and we initialize again the Split-Bregman variables $\boldsymbol{b}^{k+1}$ and $\boldsymbol{d}^{k+1}$. We remark that every time we perform the CCE step the minimization problem (2) reduces to the first term (3a) ignoring the smoothing part (3b). Concerning the implementation, we use a classical CCE algorithm [11] using a six-connected 3D image graph. In conclusion, setting the level-set equal to a connected component each N iterations, we force the whole algorithm to extract only the vascular segment of interest from the medical image.

Finally, we have to define the feature image to be given as input to our segmentation procedure. Since the method takes information mainly from the image intensity u_0, we have to ensure that the vascular segment we want to extract is characterized by the highest image intensity values and by high contrast with its background. If the medical image does not have this features, we can select a range of intensity values $[a, b]$ and set all the pixels out of the range equal to the value a. In this way, choosing b as the maximum intensity value of the region of interest and a as a value of its background, we obtain a processed image with the desired features. We call this pre-processing step *select-range*. Another problem of medical image can be the presence of noise. Despite our method, thanks to the convolution with the Gaussian kernel, works good also in case of some noise, reducing it can improve the general performance. Indeed, the presence of noise negatively affects the quality of the edge detector $g(u_0)$ (10). Moreover, if the *select-range* step is performed, some amount of noise is naturally introduced by the thresholding procedure and some subsequent smoothing is consequently

6

Table 1: Fixed Parameters of the Segmentation Method

λ_1	λ_2	ε	β	ν	α
10^{-5}	10^{-5}	10^{-5}	100	1	0.5

needed. Thus, in case of noisy images or after the *select-range* step, we filter the image with a median filter of radius equal to one pixel. Finally, the last step we perform to generate our feature image consists of a rescaling of the intensity values in the fixed range $[0, 255]$ to deal always with similar intensity values. Note that, since the function u_0 takes real values, the image does not loose any information during this step. We perform this rescaling in order to define a set of parameters that do not depend on the single medical image. Indeed, despite the number of parameters is high, we can leave most of them fixed with the values shown in Table 1, focusing only on the scale parameter σ, the Lagrange multiplier λ and the frequency $1/N$ of the CCE. We discuss more in detail the meaning of each parameter in the next section.

We conclude showing the whole algorithm of our method, underlining also the generation of the feature image just described:

1: $u_0 \leftarrow$ select-range$(u_0, [a, b])$ {in case of bad contrast}
2: $u_0 \leftarrow$ median-filter(u_0) {in case of noisy image}
3: $u_0 \leftarrow$ rescale-values$([0, 255])$
4: $\phi^0 \leftarrow \phi_0, \quad \boldsymbol{d}^0 \leftarrow \nabla\phi_0, \quad \boldsymbol{b}^0 \leftarrow \boldsymbol{0}$ {initialize variables}
5: **for** $k = 0, 1, 2, \ldots$ **do**
6:   $r^k \leftarrow \lambda_1 e_1^k - \lambda_2 e_2^k$ {using ϕ^k and eq. (4)$\rightarrow$(9)}
7:   $\phi^{k+1} \leftarrow$ solve-poisson-problem   {eq. (13)}
8:   $\boldsymbol{d}^{k+1} \leftarrow$ shrink-operator   {eq. (15)}
9:   $\boldsymbol{b}^{k+1} \leftarrow \boldsymbol{b}^k + \nabla\phi^{k+1} - \boldsymbol{d}^{k+1}$
10:   **if** $(k \bmod N$ **and** $\phi^{k+1}(P_0) > 0)$ **then**
11:    $\phi^{k+1} \leftarrow$ CCE(ϕ^{k+1}) {binary level set}
12:    $\boldsymbol{d}^{k+1} \leftarrow \nabla\phi^{k+1}, \quad \boldsymbol{b}^{k+1} \leftarrow \boldsymbol{0}$
13:   **end if**
14: **end for**

3   Results and Discussion

We apply our method on two different kind of medical images, a 3D contrast-enhanced MR image (CE-MRI) and a CT scan, and we compare the obtained results with the results of the original method proposed by [8]. In both cases our aim is to reconstruct the aorta. The first image is a CE-MRI of a patient with a dilated ascending aorta (Fig. 1); the second image is a CT of a patient with a ventricular assist device (VAD) (Fig. 2a) and we want to
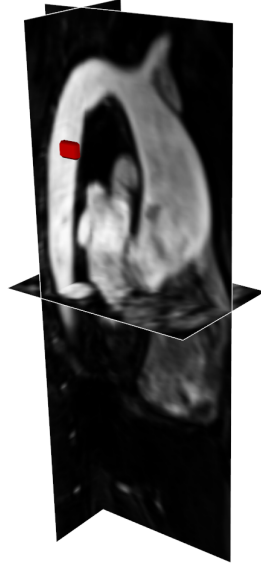
Figure 1: The CE-MRI of the patient with ascending aortic dilatation, with the initial cube in red.
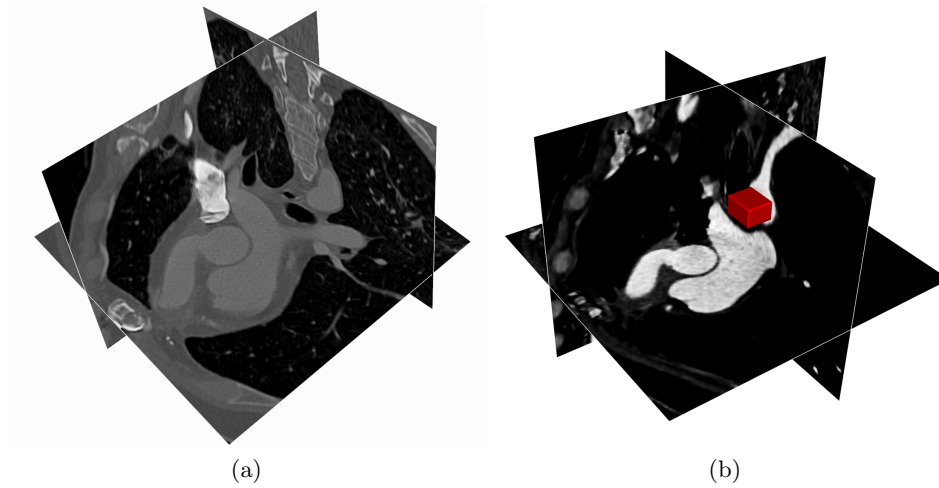

(a)

(b)

Figure 2: The original CT of the patient with VAD on the left and the resulting image after preprocessing on the right (with the initial cube in red).

segment both the aorta and the artificial cannula with the anastomosis at the beginning of the ascending aorta. The CE-MRI, thanks to the contrast agent injected in the patient, is ready for the application of our method. Indeed, the aorta has a good contrast with its background and assumes the highest image intensity values. More in detail, the image intensity values are in the range $[0, 751]$ and the aorta is characterized by values in the range $[350, 550]$ which are among the highest in the image. Concerning image resolution, the CE-MRI pixel size is $1.375\,mm \times 1.375\,mm$, while the spacing between slices is $1.5\,mm$. The CT image, instead, is characterized by intensity values in the range $[-1024, 3071]$, while the vascular segment we want to extract has values in the range $[250, 450]$ with a background of about -50. The highest value of intensity characterize, aside from the bones, the right part of the heart and circulation, where the contrast agent was located in the moment of the scan; indeed, there is no contrast agent in the aorta and in the cannula at the moment of the acquisition. Thus, we can considerer this image as a CT without contrast agent in the vascular segment of our interest (see Fig. 2a). In this case we have to pre-process the image in order to construct the correct feature image, hence the *select-range* step is performed with values $[-50, 450]$ and the median filter is consequently used. The processed image is shown in Fig. 2b: after the pre-processing steps the aorta assumes the highest intensity values as required by our method. Concerning image resolution, the CT pixel dimension is $0.771\,mm \times 0.771\,mm$, while the distance between slices is $1\,mm$.

We discuss now the meaning of each parameter involved in our method, starting from the ones that we suggest to leave fixed (Table 1). The parameters λ_1 and λ_2 weight the two functions e_1 and e_2, e.g. if $\lambda_1 > \lambda_2$ the evolution of the level set in Ω_1 is penalized. We decided to fix them equal each other since the unbalance of the two parameters has some negative consequences, i.e. the overestimation or the underestimation of the object of interest or the generation of new artificial contour inside it [9]. The parameter ε decides the accuracy of the approximation of the Heaviside function and, as a consequence, the measure of the intersection between Ω_1 and Ω_2. Setting it to a small value ensures a small overlap between the two regions, disadvantaging the attachment of near objects. The weight β beside the gradient of the intensity function u_0 in equation (10) determines the influence of the edge detector in the evolution of the level set. A big weight is suggested if the edge detector is of good quality, while a small one is better in the contrary. Since in general, when dealing with medical images, it is difficult to identify the edges only with the gradient of the intensity function, a good choice is to set β to an intermediate value. Considering the order of magnitude of each function involved in the algorithm after the automatic rescaling of u_0 in the range $[0, 255]$, the value of 100 represents a good compromise. Finally, the parameter ν can be fixed to 1 without loosing the generality of the method [8] and we suggest a value of α equal

Table 2: User Parameters of the Segmentation Method for the CE-MRI and the CT images

	σ	λ	N
CE-MRI	3.5	0.15	2
CT	4.5	0.1	2

to 0.5.

In Table 2 we report the values of the other parameters in the two different cases of the CE-MRI and CT. The scale parameter σ regulates the width of the Gaussian kernel (7) and, as a consequence, the width of the local approximation of the intensity u_0 through the two functions f_1 and f_2 (8). As a consequence, a small σ allows the segmentation of inhomogeneous images and ensures a result with a higher level of details; on the contrary, it can cause the development of new contours inside the object of interest. A good compromise is to set this parameter about an order of magnitude smaller than the diameter of the vessel we are interested to segment. Thus, in the case of the aorta, values of sigma between $2\,mm$ and $5\,mm$ are good choices, while, in the case of smaller vessels (e.g. coronaries) a much smaller σ is necessary. Finally, the Lagrange multiplier λ, since it appears as a weight in the right hand side of the equations (13), influences the quantity of diffusion at each iteration k and, as a consequence, the speed of growth of the level set ϕ. Hence, when the value of this parameter is high, the algorithm slows down and a bigger number of iterations are necessary to obtain the final result. Despite this strategy seems useless, we need to combine the CCE with a general slowing-down of the algorithm, to avoid the attachment with near objects. For this reason, we suggest to set λ about 0.1 and perform the CCE each two iterations. In case this is not sufficient to avoid the union of near objects, it is suggested to increase λ even more.

We finally show the results of our method at different iterations and on both images, comparing them with the results of the original method [8] (see Fig. 3 and Fig. 4). Note that we apply both methods to the same initial images (Fig. 1 and Fig. 2b) with the same parameters (Tables 1 and 2) and the same initializations (i.e. the red cubes in Fig. 1 and Fig. 2b). Moreover, we recall that the results of both methods can be made of more than a connected component. While in the case of our method the parts not connected with the region of interest are usually small or do not exist (because they are iteratively deleted by the CCE every two iterations), in the case of the original method they can be very large. For this reason, to be fare in the comparison, we always show only the part of the zero level of ϕ connected to the region of interest.

In Fig. 3 we report the results obtained with the CE-MRI after 5, 25 and 59 iterations for both methods. The dilated ascending aorta is very

well segmented by our method (see Fig. 3f) and, looking at the evolution of the contour (Fig. 3 (d)–(f)), it is clear that we reach the aim of avoiding the attachment with other objects. On the contrary, the corresponding results of the original method (Fig. 3 (a)–(c)) are clearly affected by the attachment of nearby vessels and organs both in the ascending and in the descending aorta resulting in an incorrect final segmentation. An analogous

(a) Iteration 5.   (b) Iteration 25.   (c) Iteration 59.

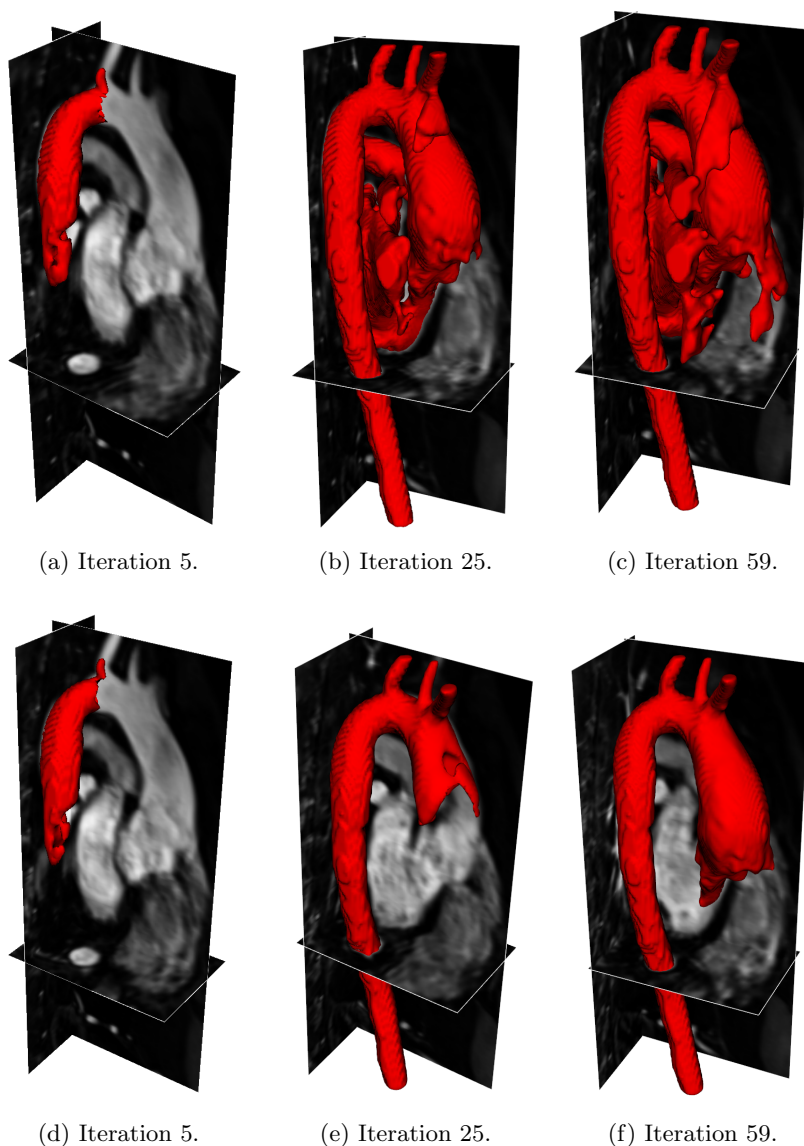(d) Iteration 5.   (e) Iteration 25.   (f) Iteration 59.

Figure 3: CE-MRI, comparison of the results at different iterations: (a)–(c) obtained with original method described in [8], (d)–(f) obtained with our method. The red surface is the connected component of the zero level of ϕ.

behavior can be seen in the second test of the CT with VAD (Fig. 4). The evolution of the contour with the original method generates a surface including also the pulmonary artery and part of the heart (Fig. 4 (a)–(e)), while our method is able to isolate only the aorta and the artificial cannula of the VAD (Fig. 4 (b)–(f)). Moreover, we note also the quality of the final segmentation (Fig. 4f), where the three sinuses of Valsalva are clearly visible and the anastomosis between the artificial cannula and the aorta is perfectly

(a) Iteration 5.   (b) Iteration 5.

(c) Iteration 15.   (d) Iteration 15.
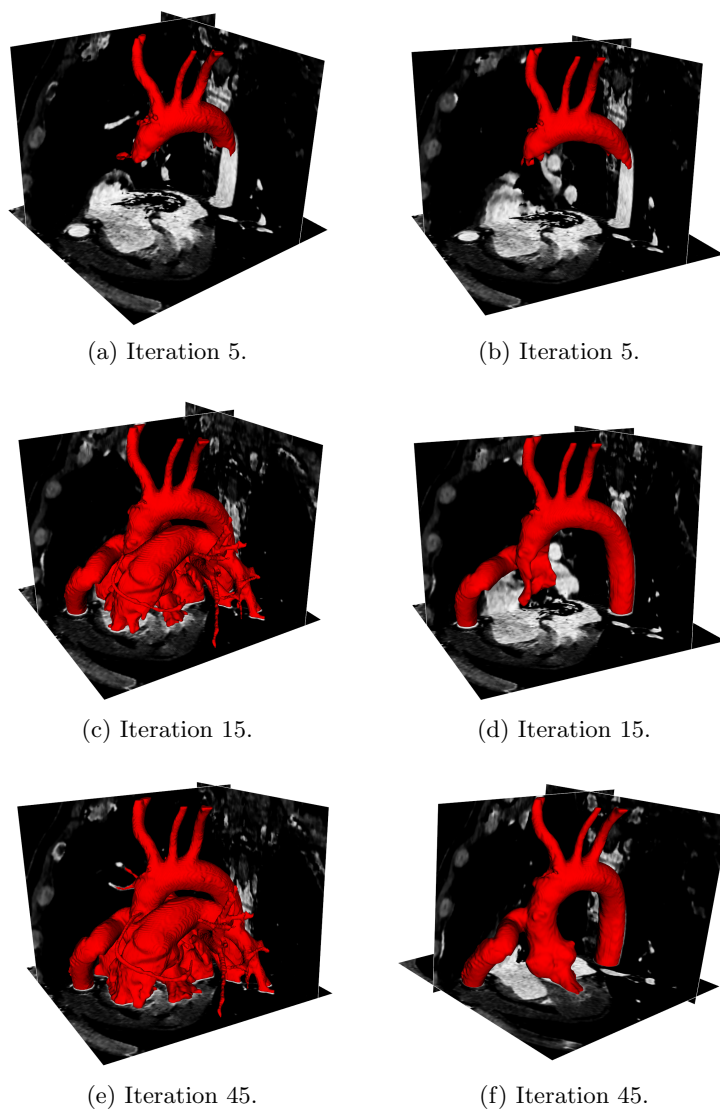
(e) Iteration 45.   (f) Iteration 45.

Figure 4: CT image, comparison of the results at different iterations: (a)–(c)–(e) obtained with original method described in [8], (b)–(d)–(f) obtained with our method. The red surface is the connected component of the zero level of ϕ.

reconstructed. Finally, we underline that these results are obtained with a minimum interaction by the user, that has only to choose the position of the initial cube.

We conclude noting that our results can be easily post-processed to perform the applications mentioned in the first section, such as patient-specific computational hemodynamics, patient-specific computational mechanics and patient-specific complex vascular morphological analysis.

4   Conclusions

In this work we develop a modification of the segmentation method proposed in [8] in order to make it suitable for the reconstruction of vascular structures from 3D medical images. The original method consists in the minimization of the RSFE functional [9] using the Split-Bregman method [10]. We modify the iterative algorithm adding a connected component extraction of the solution each N iterations, starting from a point that identifies the vascular structure of interest. In this way, we take advantages of a local constraint to focus the original region-based method only on the user-defined region of interest and, consequently, we avoid the attachment of the vascular structure with nearby objects. Finally, we suggest a strategy to limit the user interaction: we fix most of the parameters of the method, allowing the tuning of only three of them. We test the proposed method on two different kind of medical images (a MRI and a CT) reconstructing in both cases the aortic arch of two patients with complex geometries (an ascending dilatation and the ventricular assist device). The obtained results demonstrate that our method outperforms the original method in segmenting the vascular region of interest and all the important details (such as the sinuses of Valsalva, the anastomosis and the aortic dilatation) without the inclusion of nearby objects in the result (such as pulmonary branches or heart).

A limitation of our study is related to the low number of tested images; indeed, the currently available data involve vessels of relatively large size. We are planning to test the algorithm in more challenging situations with the presence of veins/arteries of relatively small diameter. Despite the obtained results are qualitatively very promising, additional studies with a larger dataset and with quantitative comparison with other methods are required.

Acknowledgment

References

[1] L. Formaggia, A. Quarteroni, and A. Veneziani, *Cardiovascular Mathematics: Modeling and simulation of the circulatory system*. Springer Science & Business Media, 2010, vol. 1.

[2] C. A. Taylor and C. Figueroa, "Patient-specific modeling of cardiovascular mechanics," *Annual review of biomedical engineering*, vol. 11, pp. 109–134, 2009.

[3] R. D. Millán, L. Dempere-Marco, J. M. Pozo, J. R. Cebral, and A. F. Frangi, "Morphological characterization of intracranial aneurysms using 3-d moment invariants," *Medical Imaging, IEEE Transactions on*, vol. 26, no. 9, pp. 1270–1282, 2007.

[4] A. Lauric, E. L. Miller, M. I. Baharoglu, and A. M. Malek, "3d shape analysis of intracranial aneurysms using the writhe number as a discriminant for rupture," *Annals of biomedical engineering*, vol. 39, no. 5, pp. 1457–1469, 2011.

[5] J. R. Cebral, M. A. Castro, J. E. Burgess, R. S. Pergolizzi, M. J. Sheridan, and C. M. Putman, "Characterization of cerebral aneurysms for assessing risk of rupture by using patient-specific computational hemodynamics models," *American Journal of Neuroradiology*, vol. 26, no. 10, pp. 2550–2559, 2005.

[6] J. R. Cebral, M. A. Castro, S. Appanaboyina, C. M. Putman, D. Millan, and A. F. Frangi, "Efficient pipeline for image-based patient-specific analysis of cerebral aneurysm hemodynamics: technique and sensitivity," *Medical Imaging, IEEE Transactions on*, vol. 24, no. 4, pp. 457–467, 2005.

[7] L. Antiga, M. Piccinelli, L. Botti, B. Ene-Iordache, A. Remuzzi, and D. A. Steinman, "An image-based modeling framework for patient-specific computational hemodynamics," *Medical & biological engineering & computing*, vol. 46, no. 11, pp. 1097–1112, 2008.

[8] Y. Yang, C. Li, C.-Y. Kao, and S. Osher, "Split bregman method for minimization of region-scalable fitting energy for image segmentation," in *Advances in Visual Computing*, ser. Lecture Notes in Computer Science. Springer Berlin Heidelberg, 2010, vol. 6454, pp. 117–128.

[9] C. Li, C.-Y. Kao, J. C. Gore, and Z. Ding, "Minimization of region-scalable fitting energy for image segmentation," *Image Processing, IEEE Transactions on*, vol. 17, no. 10, pp. 1940–1949, 2008.

[10] T. Goldstein and S. Osher, "The split bregman method for l1-regularized problems," *SIAM Journal on Imaging Sciences*, vol. 2, no. 2, pp. 323–343, 2009.

[11] P. A. Devijver, *Connected components in binary images: the detection problem.* John Wiley & Sons, Inc., 1984.

[12] T. Chan and L. Vese, "Active contours without edges," *Image Processing, IEEE Transactions on*, vol. 10, no. 2, pp. 266–277, 2001.

[13] T. Chan, S. Esedoglu, and M. Nikolova, "Algorithms for finding global minimizers of image segmentation and denoising models," *SIAM Journal on Applied Mathematics*, vol. 66, no. 5, pp. 1632–1648, 2006.

[14] X. Bresson, S. Esedolu, P. Vandergheynst, J.-P. Thiran, and S. Osher, "Fast global minimization of the active contour/snake model," *Journal of Mathematical Imaging and vision*, vol. 28, no. 2, pp. 151–167, 2007.

MOX Technical Reports, last issues

35/2015 Manzoni, A.; Pagani, S.
A certified reduced basis method for PDE-constrained parametric optimization problems by an adjoint-based approach

32/2015 Agasisti,T.; Ieva, F.; Masci, C.;Paganoni, A.M.
Does class matter more than school? Evidence from a multilevel statistical analysis on Italian junior secondary school students

33/2015 Fumagalli, A; Pasquale, L; Zonca, S.; Micheletti, S.
An upscaling procedure for fractured reservoirs with non-matching grids

34/2015 Bernardi, M.S.; Mazza, G.; Ramsay, J.O.; Sangalli, L.M.
A separable model for spatial functional data with application to the analysis of the production of waste in Venice province

31/2015 Pini, A.; Vantini, S.; Colombo, D.; Colosimo, B. M.; Previtali, B.
Domain-selective functional ANOVA for process analysis via signal data: the remote monitoring in laser welding

29/2015 Antonietti, P.F.; Cangiani, A.; Collis, J.; Dong, Z.; Georgoulis, E.H.; Giani, S.; Houston, P.
Review of Discontinuous Galerkin Finite Element Methods for Partial Differential Equations on Complicated Domains

30/2015 Pini, A.; Vantini, S.
Interval-wise testing for functional data

28/2015 Taffetani, M.; Ciarletta, P.
Beading instability in soft cylindrical gels with capillary energy: weakly non-linear analysis and numerical simulations

25/2015 Del Pra, M.; Fumagalli, A.; Scotti, A.
Well posedness of fully coupled fracture/bulk Darcy flow with XFEM

26/2015 Tagliabue, A.; Dede', L.; Quarteroni, A.
Nitsche's Method for Parabolic Partial Differential Equations with Mixed Time Varying Boundary Conditions